



HAL
open science

Modulating thermal transport in a porous carbon honeycomb using cutting and deformation techniques

Yang Han, Chaoxiang Zhao, Hao Bai, Yanjun Li, Jiayue Yang, Yi-Tung Chen,
Guo Hong, David Lacroix, Mykola Isaiev

► **To cite this version:**

Yang Han, Chaoxiang Zhao, Hao Bai, Yanjun Li, Jiayue Yang, et al.. Modulating thermal transport in a porous carbon honeycomb using cutting and deformation techniques. *Physical Chemistry Chemical Physics*, 2022, 24 (5), pp.3207-3215. 10.1039/D1CP04210F . hal-03799717

HAL Id: hal-03799717

<https://hal.science/hal-03799717>

Submitted on 6 Oct 2022

HAL is a multi-disciplinary open access archive for the deposit and dissemination of scientific research documents, whether they are published or not. The documents may come from teaching and research institutions in France or abroad, or from public or private research centers.

L'archive ouverte pluridisciplinaire **HAL**, est destinée au dépôt et à la diffusion de documents scientifiques de niveau recherche, publiés ou non, émanant des établissements d'enseignement et de recherche français ou étrangers, des laboratoires publics ou privés.

Modulating Thermal Transport in Porous Carbon Honeycomb by Cutting and Deformation Techniques

Yang Han^{1,*}, Chaoxiang Zhao¹, Hao Bai¹, Yanjun Li¹, Jiayue Yang², Yi-Tung Chen³, Guo Hong^{4,5},

David Lacroix⁶, Mykola Isaiev⁷

¹*College of Power and Energy Engineering, Harbin Engineering University, 150001 Harbin, China*

²*School of Energy and Power Engineering, Shandong University, Jinan, Shandong, 250061, China*

³*Department of Mechanical Engineering, University of Nevada, Las Vegas, NV 89154, USA*

⁴*Institute of Applied Physics and Materials Engineering, University of Macau, Avenida da Universidade, Taipa, Macau SAR 999078, China*

⁵*Department of Physics and Chemistry, Faculty of Science and Engineering, University of Macau, Avenida da Universidade, Taipa, Macau SAR 999078, China*

⁶*Universit e de Lorraine, CNRS, LEMTA, Nancy, F-54500, France*

⁷*Universit e de Lorraine, CNRS, LEMTA, Nancy, F-54000, France and Faculty of Physics, Taras Shevchenko National University of Kyiv, 64/13, Volodymrska str., 01601, Kyiv, Ukraine*

ABSTRACT

During past years, there has been a flurry of investigations on the lattice thermal transport of three-dimensional (3D) graphene, but few studies on how to adjust this property effectively by present engineering technologies. In this work, thermal transport properties of a porous single layer carbon honeycomb (SL-dCHC-2) and its mechanical response are systematically studied. We show that the thermal conductivity of SL-dCHC-2 can be adjusted effectively by varying the tensile strain, and its value for SL-dCHC-2 is enhanced up to 11.3 times with 8% strain as compared to the unstrained case. This is exceedingly larger than what was observed for other two-dimensional (2D) materials

such as silicene (~7 times larger). This outstanding behavior is explained from the phonon mode level, indicating that the profound increase of thermal conductivity under tensile strain is attributed to the enhancement of phonon lifetime. Besides, the trend of root mean squared displacement, which is closely related to phonon anharmonic effect, correlates with the non-monotonic response of the dimerized C-C bonds at the linkage of the structure. These investigations and obtained results provide important guidance to develop 3D carbon honeycomb for several purposes such as molecular sieve and water purification applications.

Keywords: Carbon Honeycomb, Thermal Transport, First-Principles Calculations, Cutting, Deformation

I. INTRODUCTION

The outstanding personalities such as the special property superiority, the wide range of applications in many fields and the vast applicate prospects have triggered an increasing worldwide tide of research on carbon based materials [1]. Investigation on physical properties of these kind of carbon structures and developing more effective techniques to modulate them has always been a hot topic in the present scientific world. As one representative of the numerous carbon honeycomb structures, three-dimensional (3D) graphene (Space group: P6/mmm with No. 191) was firstly predicted theoretically from first-principles calculations by Wu *et al.* in 2011 [2]. Then, it was successfully synthesized in experiment by Krainyukova and Zubarev via the deposition of vacuum-sublimated graphite in 2016 [3]. The newly synthesized carbon honeycomb structure with hollow channel network has many outstanding characteristics, such as high mechanical strength, large thermal conductivity, light weight and giant energy absorption capacity, making it possess great potential applications [4, 5].

Firstly, it can be used as a light and energy-efficient fuel storage medium, e.g. used in the hydrogen fuel cell as a good gas absorber [6]. In addition, 3D graphene has a large specific surface area, providing more abundant adsorption sites when used in electrochemical catalysis. Recently, Shi *et al.* has proved through DFT calculations that the 3D carbon honeycomb structure with lower atomic energy barrier can be used as an excellent nanoporous medium carrier for lithium and sodium atoms in efficient lithium battery devices [7]. It is highly expected that porous carbon honeycomb materials will be widely used in gas packaging, surface chemistry, catalysis, toxic gas filtration and water purification, *etc.*

Since the 3D graphene structure was firstly predicted theoretically, and especially synthesized experimentally in 2016, a continuous series of investigations has been implemented to this new member of 3D carbon materials. The concerned properties covered various aspects, including the debatable structure stabilities [8-14], different geometric structures from different dimerization junctions to various chirality linkages [4, 14], mechanical [2, 4, 15], thermal transport [4, 8, 9, 13, 15], electronic [2, 8], magnetic [16] and thermoelectric [10] properties.

Of these various properties, the research on thermal transport has also attracted considerable interest. For instance, Gao *et al.* investigated the lattice thermal transport properties of CHC-n using classical molecular dynamics in 2016, demonstrating that the thermal conductivity of CHC-2 is 45 times lower than that of graphene (about $4000 \text{ Wm}^{-1}\text{K}^{-1}$) [8]. In the CHC-n structure, all C atoms are sp^2 hybridized in contrast to the dCHC-n with some C atoms sp^3 -hybridized at the connection chain. In 2017, Wei *et al.* used a similar method to study the lattice thermal conductivity of CHC-n structure taking into account the pressure effect on it, providing that its thermal conductivity has strong anisotropy and its axial value decreases with the increase of pressure [9]. Then several research groups became more and more interested in the thermal transport characteristics of the stable 3D graphene model structure dCHC-n, carrying out in-depth numerical calculations in their research. First of all, Gu and Wei *et al.* calculated the lattice thermal conductivity of dCHC-n structures with different porous channel sizes by implementing classical molecular dynamics (MD) simulations [4, 15]. Later on, first-principles calculations combined with phonon Boltzmann transport equation (BTE) were employed to study the lattice thermal transport properties of dCHC-2 structure, obtaining the lattice thermal conductivity value of $\sim 150/24 \text{ W/(mK)}$ in the direction parallel/perpendicular respectively to

the hole axis [13], which is lower than the ones from the previous classical MD simulations [4]. In this framework, we have also studied the strain influence on the thermal transport performance of dCHC-2 structure based on the first-principles calculations. We show that the lattice thermal conductivity increases abnormally with the structure volume expansion [13]. As discussed above, in the recent years there has been a lot of investigations on the lattice thermal transport of 3D graphene but few on how to adjust this property effectively.

As is well known that the number of material layers, commonly called dimensionality, has a great influence on transport properties. For example, using the linearized Boltzmann transport equation and perturbation theory, Singh *et al.* compared the thermal transport properties of single layer (SL) graphene with its bulk counterpart graphite [17]. They analyzed the reduction of the intrinsic thermal conductivity of few-layer graphene sheets, considering all possible three phonons scattering events. Their results revealed that even with weak coupling between layers, a significant degradation in the thermal conductivity due to the out-of-plane acoustic modes was apparent and the main effect of this weak coupling was to open many new three-phonons scattering channels which were otherwise absent in single layer graphene. Besides, the 3D graphene networks were already cut into slabs to generate a new class of Weyl semimetals in the recent work by DFT calculations [18].

On the other hand, in the practical applications, the materials more or less suffer different strains, leading to changes of the geometric structure, which will thus affect their physical properties such as heat transfer characteristic. Therefore, the study of strain effect on the material properties is not only of significance in important basic research, but also provides a possible way for the elaboration of

functional materials with tunable properties [19].

Considering that the dimensionality and strain are popular ways of tuning physical properties of materials, in this work, we have studied the thermal transport properties of porous single layer carbon honeycomb and its tensile response. We applied mechanical strain to mimic the structural deformation existing in molecular sieves, energy storage and catalysis [6, 7] and further investigated its influence on thermal transport based upon the first-principles lattice dynamics. The obtained results will be useful to make 3D carbon honeycomb's compounds useful in applications such as molecular sieve and in water purification equipment.

II. SIMULATION MODEL AND COMPUTATIONAL METHOD

A. Model and Geometric Optimization

Single layer 3D carbon honeycomb (SL-dCHC-n) was cut from the corresponding bulk structure dCHC-n [13] in the direction perpendicular to the channel axis. In the formed SL structure, only one pair of carbon atoms with sp^3 -hybridization at the junction is kept. As an illustration, the geometric structures of both bulk dCHC-2 and SL-dCHC-2 are shown in Fig.1 for comparison. The structure of SL-dCHC-2 retains its bulk structure similarity but also featured by some new properties due to low dimensional cutting, dangling bonds formed and newly imported surface atoms and bonds. For example, the most sensitive edge bond formed due to cutting shrunk from 1.51 Å in its bulk counterpart to 1.27 Å in SL-dCHC-2. Behavior of all representative bonds and angles in SL-dCHC-2 under strain will be discussed later elaborately.

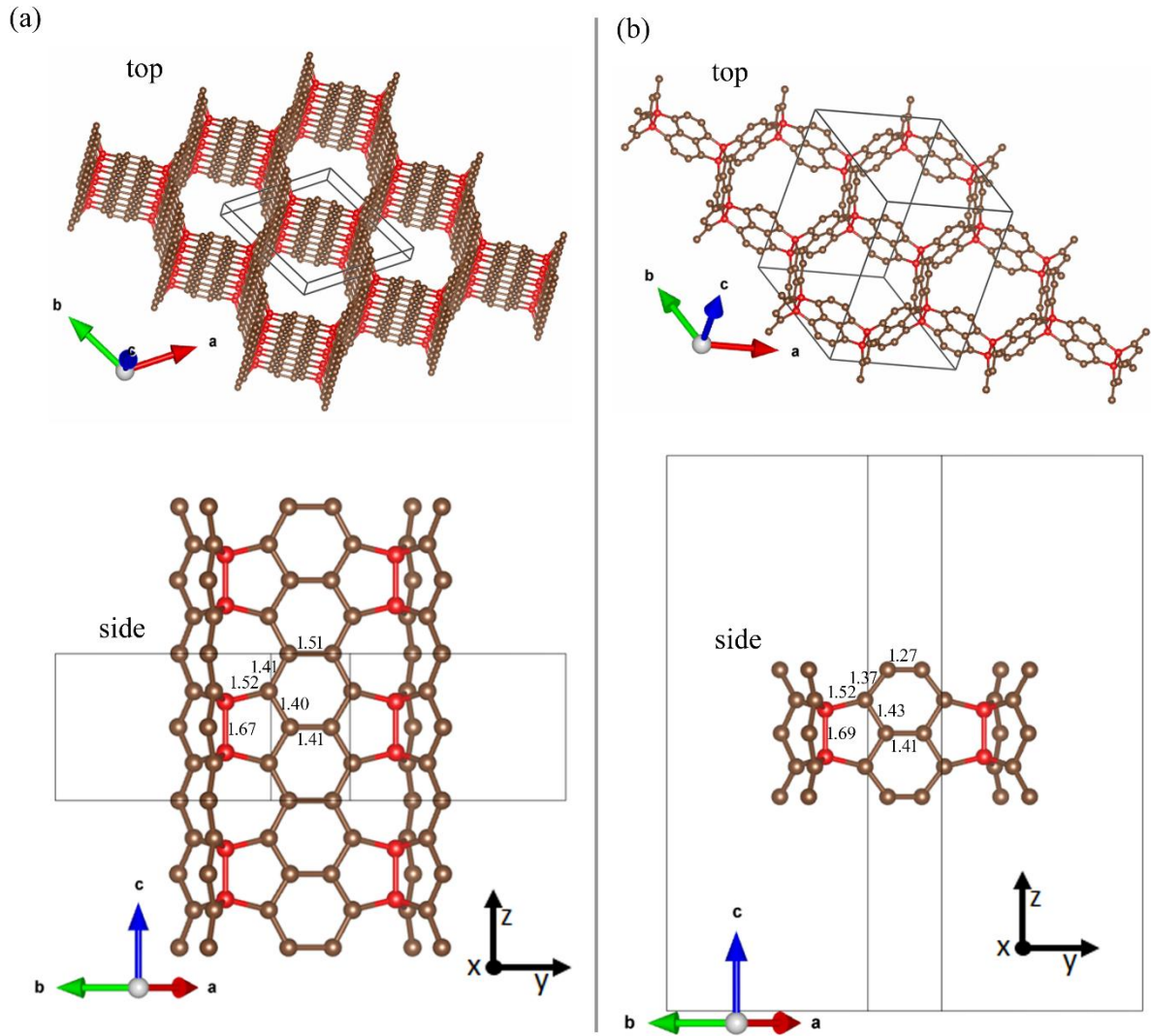


Figure 1. Top and side views of (a) bulk dCHC-2 and (b) SL-dCHC-2. The C atoms with sp^3 hybridization at the linkage are in red color for distinction, with all the representative bond lengths are also denoted. The black rhombus shows the primitive cell.

Density functional theory (DFT) calculations were employed in the generalized gradient approximation (GGA) with the Perdew–Burke–Ernzerhof (PBE) exchange–correlation [20, 21], as implemented in the Package VASP [22], in which the projected augmented wave (PAW) method [21, 23] was adopted. A kinetic energy cutoff of 600 eV was employed for the plane-wave basis set. The

$2s^23p^2$ orbitals of the C atom were treated as valence ones. We utilized a sufficient dense Monkhorst-Pack [24] k -point mesh for the summation in the first Brillouin zone (BZ). All atoms and the simulation boxes in lateral directions (the xy -direction where the plane lies) were fully relaxed, keeping box in the z direction (also along lattice c direction) restrained with a vacuum layer size equal or larger than 20 Å. Geometric structure optimizations were performed by using the conjugate-gradient algorithm [25] with a maximum residual force of 10^{-5} eV/Å at each atom. The allowed error in total energy for the electron self-consistent loop was 10^{-8} eV. The structure here we studied is a quasi-two dimensional single layer structure lying in xy plane with a finite short thickness in z direction. For the two dimensional structure, usually strain was loaded in the in-plane directions to investigate the mechanical response of its physical properties. As for the strain effect, in this work only the tensile strain (isotropic in the two lateral directions) was considered in order to mimic the expansion effect while the structure is used as molecular sieves and in the field of energy storage and catalysis. For the isotropic strain, when the specific strain was loaded in the xy -direction, the size of the box in the z direction was restrained at 20 Å with enough vacuum space between the two adjacent layers.

B. Mechanical and Thermodynamic Stability

Firstly, mechanical stability of free standing ($\epsilon = 0\%$) SL-dCHC-2 and its structure under strain ($\epsilon > 0\%$) was checked from its phonon dispersion curve by solving the eigenvalues of the dynamical matrix constructed from the harmonic force constants. The results show that there is no imaginary frequency in the phonon dispersion curve of SL-dCHC-2 for strain up to $\epsilon = 14\%$, indicating that SL-dCHC-2 under strain $\epsilon \leq 14\%$ is mechanically stable. The phonon dispersion of unstrained SL-dCHC-2 at $\epsilon = 0\%$ and $\epsilon = 8\%$ are depicted in Fig. 2 as examples.

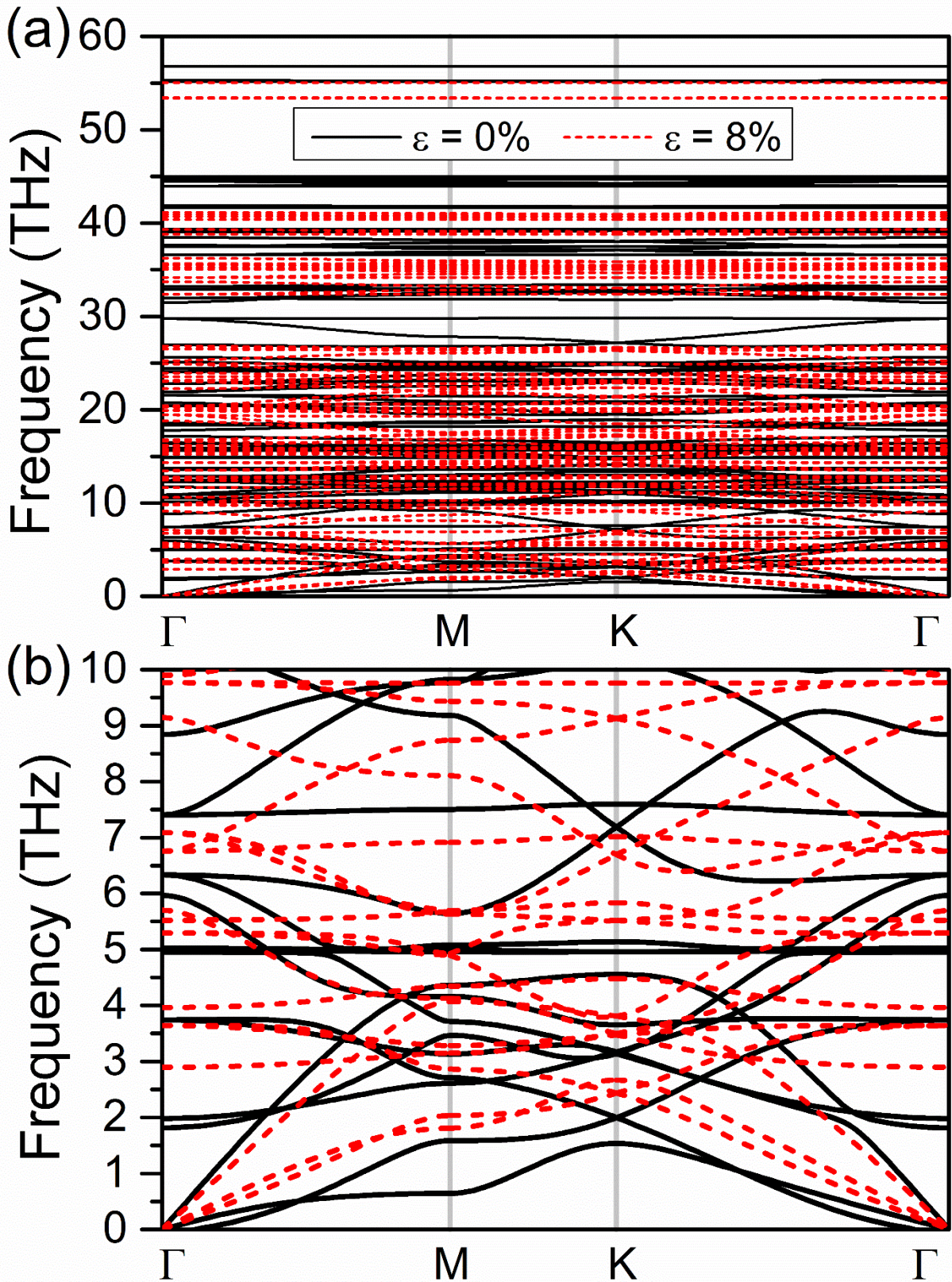


Figure 2. (a) Phonon dispersions of SL-dCHC-2 at strains of 0% and 8%, respectively, and (b) there zooms out at lower frequency range of 0 ~ 10 THz.

Besides, the thermodynamic stability of SL-dCHC-2 structure was also checked by *ab initio* molecular dynamics (AIMD) simulation at 1000 K for 10 ps. Here a relatively large ($2 \times 2 \times 1$) supercell (136 atoms in total) was used to prevent pseudo-stability caused from a smaller unit cell. Both of the temperature and energy quantities reached the thermal equilibrium state as can be seen in Fig. 3 in which the final structure was also shown as an inset.

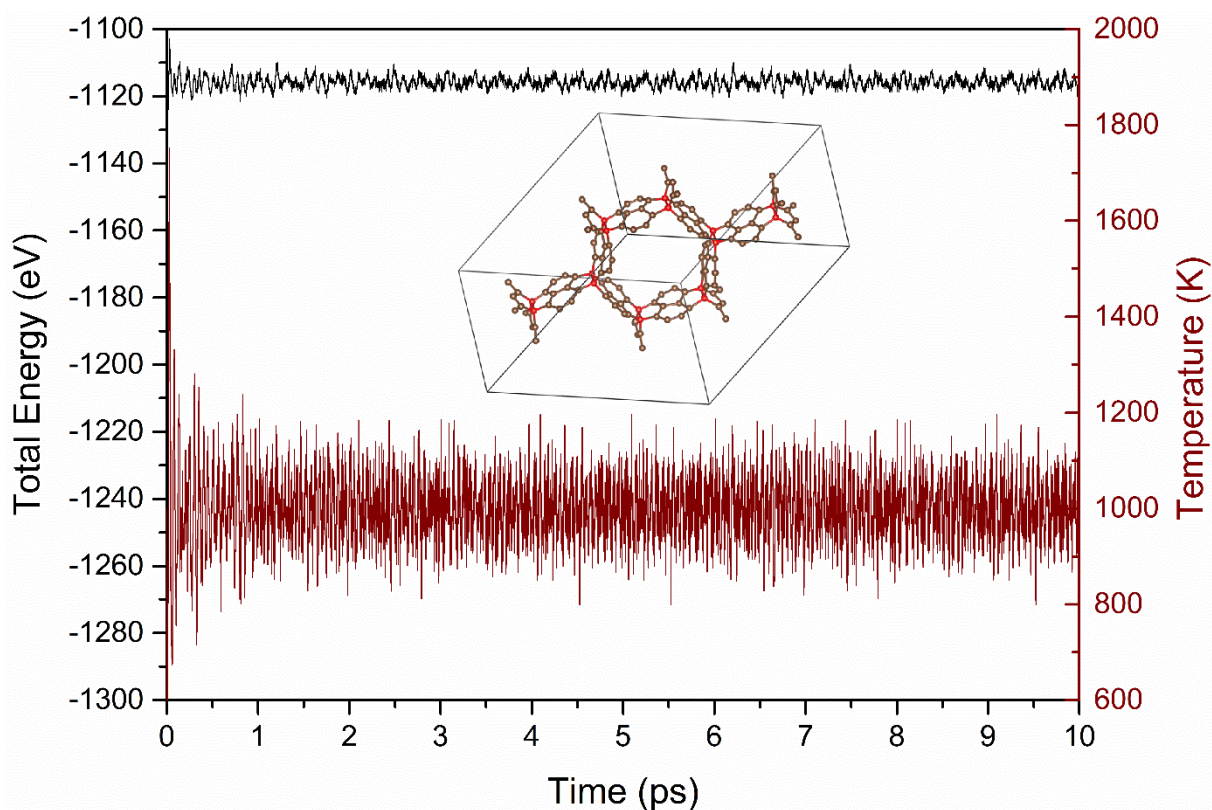


Figure 3. Energy (left axis in black) and temperature (right axis in wine) vs. simulation time during AIMD simulation for the SL-dCHC-2 structure. (Inset) The corresponding structure at the end of simulation (10 ps).

C. Thermal Conductivity Calculation

In the ShengBTE package [26], the intrinsic lattice thermal conductivity was calculated by

solving the semi-classical phonon Boltzmann transport equation (BTE) iteratively. Phonon-phonon scattering including N and U processes were considered. We utilized a $2 \times 2 \times 1$ supercell containing 136 atoms for calculating the harmonic and anharmonic IFCs with a Monkhorst-Pack [24] k -point meshes of $1 \times 1 \times 1$ to sample the BZ for SL-dCHC-2. By employing density functional perturbation theory (DFPT) in the linear response framework [27], we obtained the harmonic second-order interatomic force constant (2nd IFC) from calculating the dynamical matrix via the linear response of the electron density. Phonopy code was used to get the phonon dispersions from the harmonic IFCs [28]. But for the anharmonic third-order interatomic force constant (3rd IFC), the convergence number of the nearest neighbors are tested and finally taken to be 11th. Besides, we also tested the convergence of k -point grid in BZ for solving BTE. Here in this work, we concentrate only on the thermal conductivities at room temperature (300 K).

III. RESULTS AND DISCUSSIONS

A. Thermal Conductivities under Strain

The structure deformation is supposed to have great influence on the thermal transport properties. Our calculations showing this effect are given in Fig. 4. In the latter it is found that the thermal conductivity κ of SL-dCHC-2 exhibits a sharp increase with strain load in the xy -direction. As strain increases from 0 to 8%, the κ of SL-dCHC-2 is greatly enhanced and reaches a maximum at $\varepsilon = 8\%$. For instance, the room-temperature κ perpendicular to the honeycomb axis (the xy -direction) significantly increases from $34.3 \text{ Wm}^{-1}\text{K}^{-1}$ at zero strain to $389.1 \text{ Wm}^{-1}\text{K}^{-1}$ (11.3 times larger) at 8% strain. After that, the κ of SL-dCHC-2 decreases as the strain is further increased up to 14%.

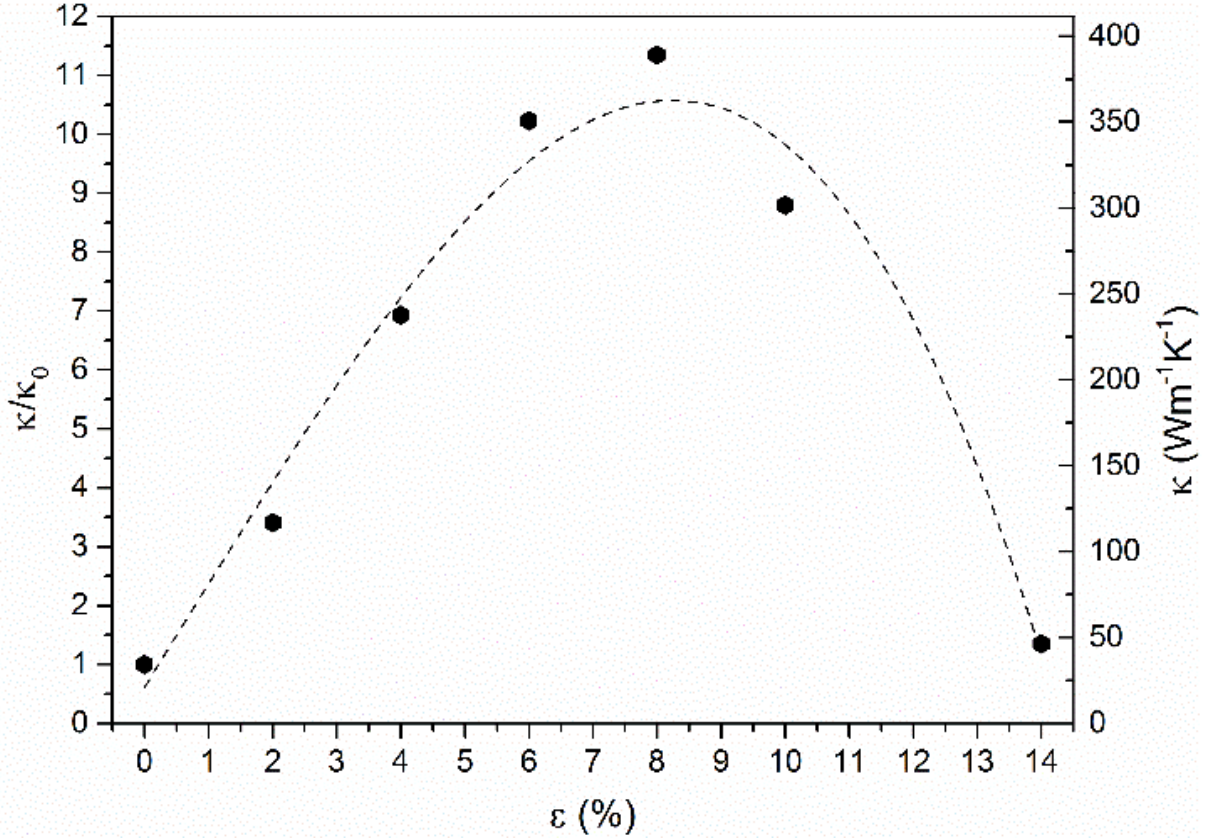


Figure 4. The strain dependent lattice thermal conductivity κ of SL-dCHC-2 structure under strain along the xy -direction (right axis) and the corresponding normalized values (left axis). The spline line is to guide the eye.

The unusual strain dependent lattice thermal conductivity κ of SL-dCHC-2 structure is very similar to that of the strained 2D silicene for which κ has a strong correlation with the buckling distance [29]. In free standing case, κ of silicene is $36.2 \text{ Wm}^{-1}\text{K}^{-1}$ from the iterative method which is slightly higher than that of SL-dCHC-2 ($34.3 \text{ Wm}^{-1}\text{K}^{-1}$). The highest thermal conductivity value of silicene appears at 4% strain and is about 7 times that of the unstrained case which is much less than that of SL-dCHC-2 (at 8% strain, 11.3 times). For graphene, the similar method indicates that κ slightly increases under tensile strain [30]. The anomalous behavior of κ of all these 2D structures under strain is obviously different with that of 3D materials. Usually the thermal conductivity values of bulk silicon

[31, 32] and diamond [33] slightly decrease under strain.

Compared to its bulk counterpart dCHC-2 which exhibits anisotropy in thermal transport along three directions, thermal energy can only transport along the xy -direction inside the single layer structure SL-dCHC-2. For the bulk case, κ also changes anomalously for strain applied in the xy -direction, similarly to that of the xyz -direction strain but with a smaller amplitude [13]. For strain only applied along the z -direction, the amplitude of κ changes continuously with increasing strain. Thus, it was concluded that the strain along the xy direction mainly contributes to the anomalous change of κ in dCHC-2, while the z -direction strain is the key to altering its amplitude. Here an interesting question about the large difference of κ increasing rates for the single layer ‘SL-dCHC-2’ under strain in the xy -direction (11.3 times larger) and bulk 3D graphene structure ‘dCHC-2’ under strain in the xy -direction (1.38 times larger) could be naturally answered. As aforementioned that strain along the xy -direction mainly contributes to the anomalous change of κ in dCHC-2, κ in SL-dCHC-2 would increase more significantly due to the absence of atomic interactions between layers in the z direction. The comparison of κ at strain in between SL-dCHC-2 and other classical structures are finally summarized in Tab. 1. Further explications to these observations are provided later when analyzing the impact of applied strain on phonon properties (group velocities and lifetime).

Table. 1 κ of different structures including SL-dCHC-2, bulk dCHC-2, silicene and silicon/diamond without strain ($\epsilon = 0\%$), critical strain (%) at which κ reaches its peak value and times κ enlarged.

Structure	SL-dCHC-2	bulk dCHC-2 [13]	silicene [29]	Bulk silicon/ diamond [31-33]
κ ($\epsilon = 0\%$)	34.3	148.15	36.2	-
Critical strain (%)	8	3	4	-
Times enlarged	11.3 (\uparrow)	1.7 (\uparrow)	~ 7 (\uparrow)	\downarrow

B. Accumulated Thermal Conductivities under Strain

To understand the anomalous response of phonon transport in the SL-dCHC-2 under strain, we firstly compute the accumulated κ versus phonon frequencies to identify which phonon frequency range provides the main contribution to the total κ of the strained SL-dCHC-2 structure. In Fig. 5(a), it is firstly found that the accumulated κ curves reach 90% of the total κ values at 6.0, 1.4 and 1.2 THz for 0, 8% and 14% strains respectively. Here low-lying acoustic phonons dominate and mostly contribute the overall κ values. Under strain, those low frequency phonons contribute significantly to the total thermal conductivity, which could ascribe to the larger and larger phonon lifetime under strain as can be seen from Fig. 6(b). Above 10 THz, at room temperature phonons do not contribute anymore to thermal transport whatever the applied strain is.

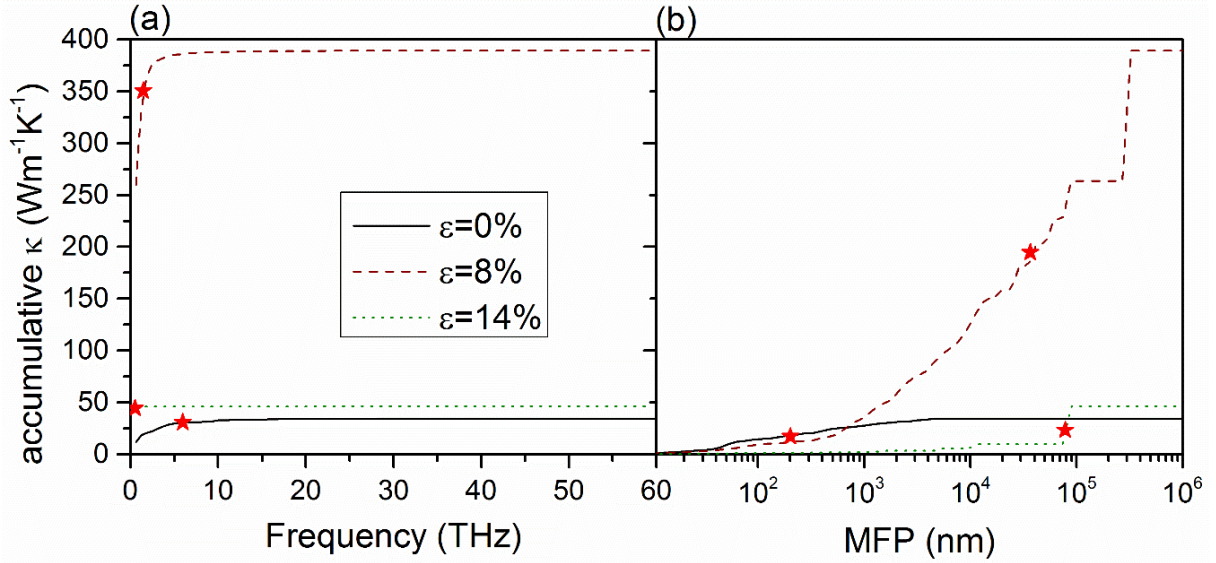


Figure 5. The accumulated lattice thermal conductivity of SL-dCHC-2 versus (a) phonon frequency and (b) phonon mean-free-path (MFP) for some typical strains: 0% in black solid, 8% in wine dashed and 14% in olive dotted lines, respectively. The red solid stars denote the frequencies (MFP), below which the phonons contribute 90% (50%) of the overall thermal conductivities.

The accumulative thermal conductivity vs. the phonon mean free path (MFP) is plotted in Fig. 5 (b). It is found that the phonons with mean free paths smaller than $\text{MFP}_{50\%} = 200.5 \text{ nm}$ contribute nearly half (50%) to the total thermal conductivity of SL-dCHC-2 without strain ($\varepsilon = 0\%$). In other words, to tailor heat dissipation performance in order to further increase/decrease thermal transport ability, such a characteristic length could provide a valuable reference for the typical size of nanostructure design. When the structures are loaded with applied strain in the xy -direction up to 8% and 14%, $\text{MFP}_{50\%}$ values are observed to increase to as much as $36.8 \mu\text{m}$ and $78.4 \mu\text{m}$, respectively. From the structural point of view, SL-dCHC-2 is composed of units of graphene nanoribbons connected together by a junction as shown by red color in Fig. 1. From an intuitive point of view,

phonons can transport along inside the ribbon parts until they are scattered when they reach the junction parts. Thus, we can suppose, as strain is loaded, the distance between adjacent junctions is enlarged, which means that phonons can be transported further before next scattering event than in the free-standing case.

C. Mode Analysis of Strain Modulated Thermal Conductivities

To get deeper in the analysis we focus further our study on this spectral range by computing the mode group velocities and phonon lifetimes. Fig. 6 (a) shows that the mode group velocity slightly decreases as the strain is enhanced from 0 to 8%, then to 14%, especially for phonons frequency in the range of 0-6 THz. This is coherent with modification observed in the phonon dispersion curves under strain. When strain is applied, some low-lying acoustic phonon branches become flattened, and thus the group velocities are decreased. This behavior cannot explain TC enhancement for applied strain of 8% as reduced group velocities implied lower TC. However, for the phonon lifetime trends are different. It exhibits anomalous change while strain increases from 0 to 8%. For phonons frequency in the range of 0-6 THz, in Fig. 6 (b), it is observed that the phonon relaxation time τ is enlarged for applied strain between 0 to 8%, but then it is reduced for strain increased from 8% to 14%. Based on this, it can be concluded that the anomalous change of phonon lifetime is the defining factor to interpret the thermal transport behavior of SL-dCHC-2 under strain. In addition, we can discuss the Umklapp process of phonon-phonon interaction importance in strained SL-dCHC-2 thermal transport. From Debye-Callaway model for calculating lattice thermal conductivity the Umklapp phonon-phonon scattering rate is proportional to the square power of the Grüneisen parameter [34]. From Fig. 6(c), we can see an obvious decrease in the amplitude of the Grüneisen parameter also its

square γ^2 as the strain goes up from 0 to 8%, indicating that the Umklapp phonon–phonon scattering is weakened.

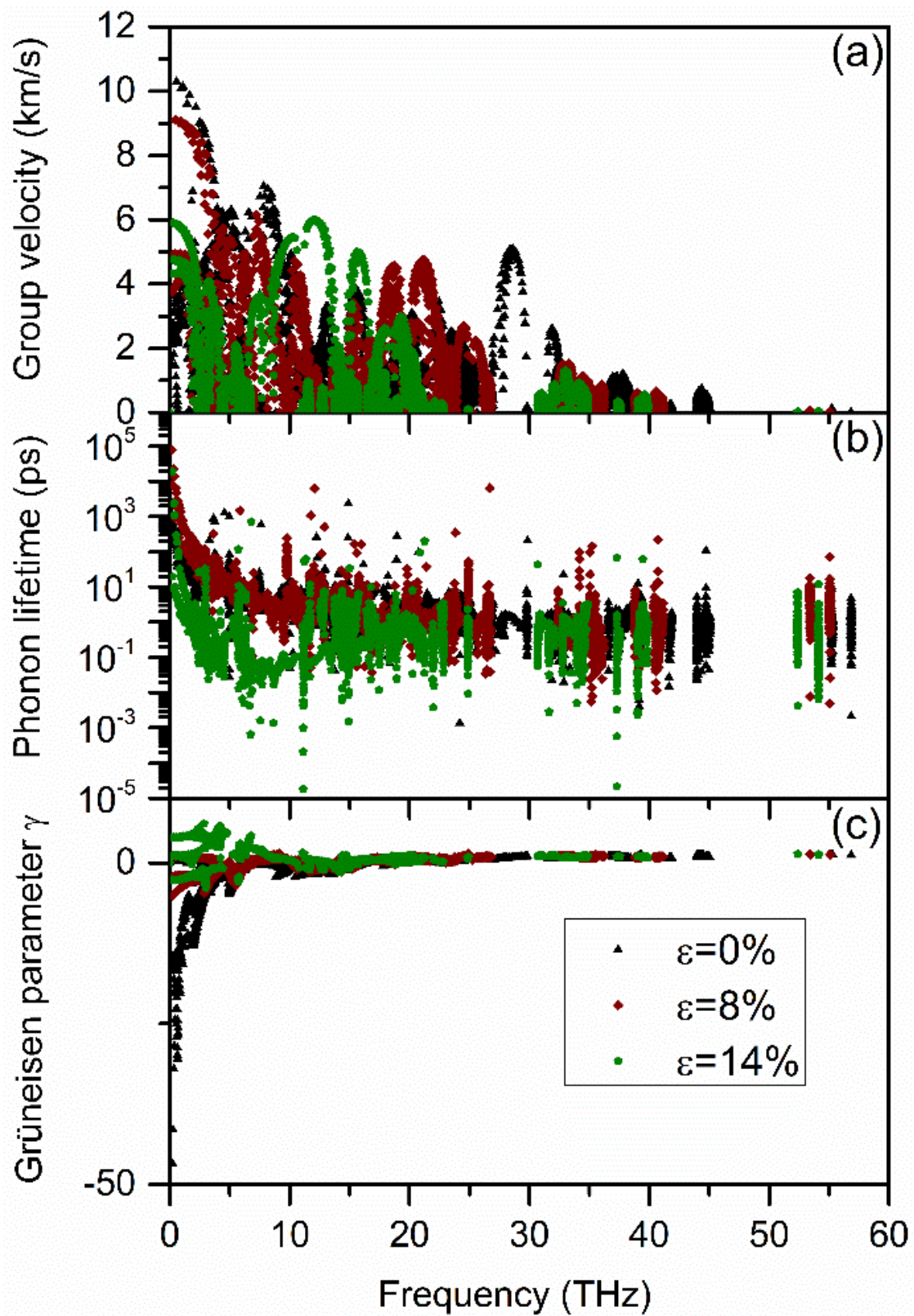


Figure 6. The phonon mode dependent (a) square group velocity, (b) phonon relaxation lifetime and (c) Grüneisen parameter γ of SL-dCHC-2 structure under some typical strains: 0% in black up triangles, 8% in wine diamonds and 14% in olive pentagons, respectively.

D. Phonon Anharmonicity Reflected from Root Mean Squared Displacement

To further explore the physical mechanism behind the phonon lifetime dependence of the thermal conductivity of SL-dCHC-2 under strain, we analyzed the root mean-square (RMS) displacement [35] which can help quantify the phonon anharmonic effect [31]. The calculated RMS values for the SL-dCHC-2 strained in the xy -direction are shown in Fig. 7. The trend of RMS is justly opposite to that of the thermal conductivity (Fig. 4), showing that the anharmonicity trend agrees well with that of the RMS.

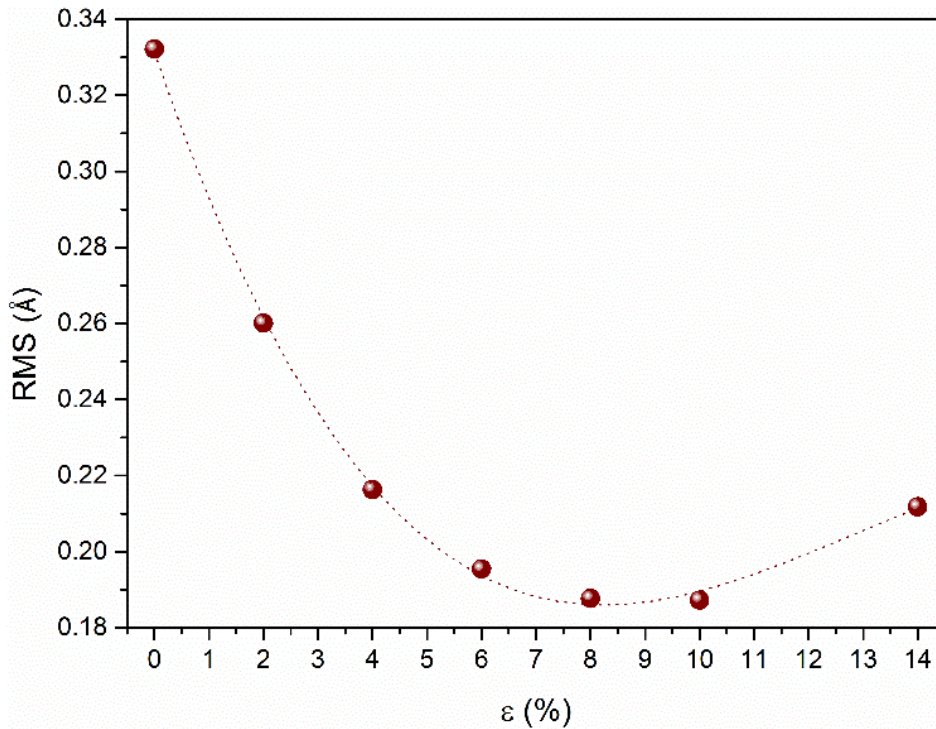


Figure 7. The root mean squared displacement of SL-dCHC-2 as a function of strain. The spline line is the guide for the eyes.

For the purpose of elucidating the phonon anharmonicity in the strained SL-dCHC-2 from detail, we then investigate the change of their typical geometric parameters (bond lengths and bond angles) with strain (see Fig. 8). It's found that, only the bond a and angles α , β and γ , correlated with the dimerized C-C linkage lines (red carbons in Fig. 1), change non-monotonically with strains, in contrast to all other geometric parameters which change monotonically. This implies that the non-monotonic strain dependence of thermal conductivity for the SL-dCHC-2 should be mainly caused by the change of the bond a at the dimerized C-C linkage line, as was similar with the case of its bulk counterpart dCHC-2 [13].

From the inset in Fig. 8(b), the non-monotonic change of the bond a at the linkage (black line with solid squares in Fig. 8(a)) could be explained reasonably from the corresponding non-monotonic variations of all the three representative bond angles $\angle\alpha$, $\angle\beta$ and $\angle\gamma$ vs. strain presented in Fig. 8(b). From Fig. 8(b), we can see that angles $\angle\alpha$ and $\angle\gamma$ go up first and then down along with strain applied, just having an opposite trend compared with that of angle $\angle\beta$. Without considering the lengths changing of bonds from b to f at the moment, increasing of angles $\angle\alpha$ and $\angle\beta$ helps elongate bond a , but angle $\angle\gamma$ does the opposite. In fact, due to the formula of $\angle\beta+2\angle\gamma=360^\circ$, trend of $\angle\beta$ change is always opposite to that of $\angle\gamma$. As can be analyzed from Tab. 2, there is a competing mechanism between angles $\angle\alpha$, $\angle\beta$ and $\angle\gamma$ contributions to the change of bond a . As a result, for the 1st part of going up trend of a , the positive contribution from increasing of angle $\angle\alpha$ plays a dominant role. Then for the 2nd part of getting down trend of a , the negative contribution from the decreasing of angle $\angle\alpha$ dominates again. It is noticeable that all bond lengths couldn't restrain constant at strain, causing that

angles of $\angle\alpha$, $\angle\beta$, $\angle\gamma$ and bond a can't strictly reach the maximum peak values at the same strain extent and thus forming a transient region as shown by a shadow in Fig. 8. In the middle of the transient region ($\varepsilon = 8\%$), thermal conductivity vs. strain reaches its inflection point as shown in Fig. 4.

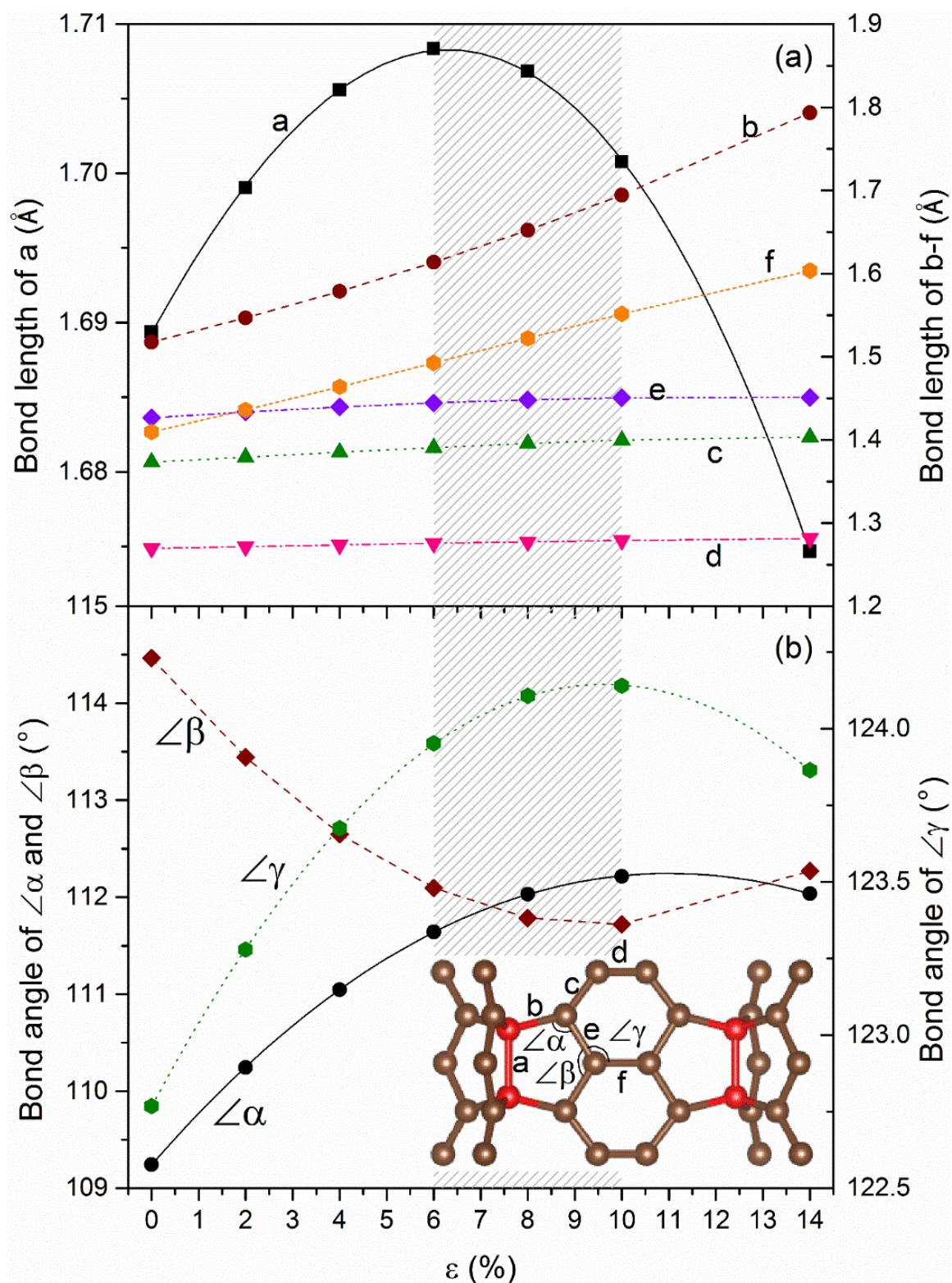


Figure 8. The typical geometric structure parameters, (a) bond length and (b) bond angle, of SL-dCHC-2 vary with different strains. Here, the lines are to guide the eye. The bonds and angles of the structure are labeled in the inset. The transient region of geometric parameters changes vs. strain from 6% to 10% has been colored in shadow.

Table. 2 The relationship between trends of the three representative bond angles $\angle\alpha$, $\angle\beta$, $\angle\gamma$ and linkage bond length a change versus strain. In the table, $\uparrow(\downarrow)$ indicates going up (down) trend and $+$ ($-$) means the parameter is positively (negatively) related to the change of bond length a .

Parameters	$\angle\alpha$	$\angle\beta$	$\angle\gamma$	a
Trend (1 st part)	$\uparrow(+)$	$\downarrow(-)$	$\uparrow(-)$	$\uparrow(+)$
Trend (2 nd part)	$\downarrow(-)$	$\uparrow(+)$	$\downarrow(+)$	$\downarrow(-)$

E. Phonon Fat Bands and Atomic Vibration Mode Contribution Analysis

Phonon vibrations are directly and closely related to lattice thermal conductivities. To explain the physical mechanism leading the thermal conductivity of SL-dCHC-2 increase first as strain goes from zero to 8% and then decrease under larger strains, the phononic k.p theorem [36, 37] is used to sort the phonon branches according to the continuity of their eigenvectors, and the line widths of the fat bands are scaled by the amplitudes of specified vibrations, as shown in Fig. 9. This technique has been widely used to analyze the atom-phonon correlation in previous studies [38-40]. Here, we only consider some representative contribution. From the structure aspect, SL-dCHC-2 is composed of graphene nanoribbons connected at junctions with each ribbon atom classified into 3 types as shown in the inset of Fig. 9: linkage atoms in red color, body atoms in green color and surface atoms in blue color, respectively. As for different types, the average partial contribution of each atom in each phonon mode

are overlaid on the total phonon dispersion.

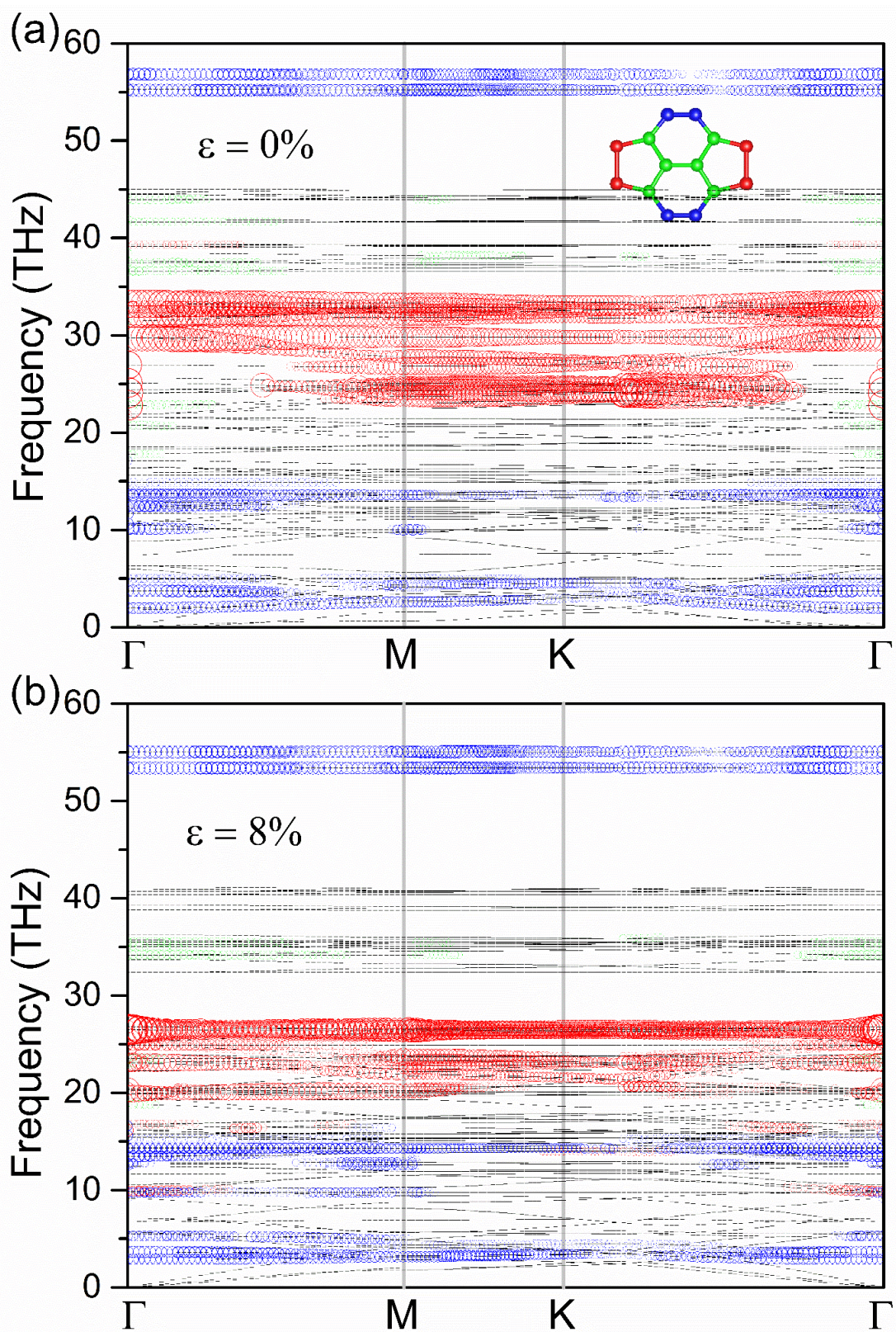


Figure 9. Phonon fat bands (black dashed line) of SL-dCHC-2 at different strains of (a) $\epsilon=0\%$ and (b) $\epsilon=8\%$.

The bubble sizes of the fat bands are scaled by the amplitudes of specified vibrations. To show clarity and brevity, here, only modes with value of average partial contribution larger than 5% are overlaid by bubbles in different colors corresponding to different partial atoms as indicated in the inset.

Firstly, we can see from Fig. 9(a) that linkage, body and surface atoms contribute to almost separate frequency regions in the whole phonon frequency range for the structure at zero strain. For details, surface atoms in blue color are responsible for phonons at the lowest and highest frequency ranges such as 0~15 THz and frequency higher than 50 THz. Linkage atoms shown by red color play an important role for the phonons in the middle frequency region 22~35 THz. And body atoms dominate the other frequency region. Compared to its bulk counterpart, the most representative geometric characteristic of SL-dCHC-2 is the two surfaces formed by cutting. So that's why the surface atoms dominate the lowest phonon frequency region which contribute mostly to the overall thermal conductivity of the layered structure. They also contribute mainly on the highest frequency region where two sets of localized bands settled due to the edge effects.

Compared to phonon fat-bands of SL-dCHC-2 at zero strain (Fig. 9(a)), the situation at 8% strain is a little bit more complicated as depicted in Fig. 9(b). Space distribution characteristic of atomic vibrational contribution analyzed above are nearly all kept, i.e. linkage atoms contribute mainly in the middle frequency region and surface atoms dominate the lowest and highest frequency regions. But differently, the three parts contributions are more mixed together. This mixing could ascribe to the geometric deformation due to strain loaded in the xy -direction. Owing to the Poisson's effect, the structure will shrink in the z -direction when it is strained in the xy -direction, leading to shortening of

distances between atoms in that direction and strengthening of atomic interactions. Even though it still exists that almost only the edge (surface) atoms dominate at the highest frequency region larger than 50 THz for the structure at the strain of $\varepsilon = 8\%$.

IV. SUMMARY AND CONCLUSIONS

In summary, we have systematically investigated thermal transport properties of single layer 3D carbon honeycomb and its mechanical response under an in-plane isotropic tensile strain by solving the Peierls-Boltzmann transport equation with interatomic force constants calculated from First-Principles. Further, a comparative study was executed on phonon dispersions and phonon vibrational modes analysis. It is fascinating to find that the thermal conductivity of SL-dCHC-2 could be adjusted effectively by tensile strain. For example, the lattice thermal conductivity of SL-dCHC-2 at zero strain ($34.3 \text{ Wm}^{-1}\text{K}^{-1}$) is enhanced to 11.3 times larger at 8% strain ($389.1 \text{ Wm}^{-1}\text{K}^{-1}$), which is drastically larger than those of other 2D materials, e.g., the well-known silicene (~ 7 times larger). By comparing the key factors of thermal conductivity at the phonon mode level, it is found that the profound increase of thermal conductivity in SL-dCHC-2 under tensile strain is dominated by the enhancement of phonon lifetime. The governing physics behind this vast increase is further unraveled in depth to be the decrease of the root mean-square displacement values, caused mainly by the non-monotonic response of the dimerized C-C bonds at the linkage of the structure. Finally, phonon vibrational modes contribution analysis was done, indicating that the surface atoms contribute mainly to the thermal conductivity at lower frequency range. Our results provide important insights into the response of thermal transport in single layer 3D carbon honeycomb upon external tensile strain,

mimicking the effect of structural deformation upon gas molecular sieving process, and offer useful guidelines for the thermal management in relevant chemical applications.

CONFLICTS OF INTEREST

There are no conflicts of interest to declare.

ACKNOWLEDGEMENTS

The authors acknowledge financial support from the National Natural Science Foundation of China with No. 51909046 and 12104111, the Fundamental Research Funds for the Central Universities (3072020CFJ0302, HEUCFG201819 and 3072020CFT303), the research fund of University of Macau, Macau SAR (File no. MYRG2018-00079-IAPME, MYRG2019-00115-IAPME), and the Science and Technology Development Fund, Macau SAR (File no. 081/2017/A2, 0059/2018/A2, 009/2017/AMJ). We are grateful for computational resources support from the High-Performance Computing Center of Collaborative Innovation Center of Advanced Microstructures and the High Performance Computing Center of Nanjing University. Y. Han gratefully acknowledges fruitful discussions with Dr. Prof. Jinming Dong (Nanjing University).

REFERENCES

- [1] Zhang Y, Ma J, Wei N, Yang J, Pei Q-X. Recent progress in the development of thermal interface materials: a review. *Physical Chemistry Chemical Physics*. 2021;23(2):753-76.
- [2] Wu M, Wu X, Pei Y, Wang Y, Zeng XC. Three-dimensional network model of carbon containing only sp²-carbon bonds and boron nitride analogues. *Chemical Communications*. 2011;47(15):4406-8.
- [3] Krainyukova NV, Zubarev EN. Carbon honeycomb high capacity storage for gaseous and liquid

species. *Physical Review Letters*. 2016;116(5):055501.

[4] Gu X, Pang Z, Wei Y, Yang R. On the influence of junction structures on the mechanical and thermal properties of carbon honeycombs. *Carbon*. 2017;119:278-86.

[5] Yi L, Chang T, Feng X-Q, Zhang Y, Wang J, Huang B. Giant energy absorption capacity of graphene-based carbon honeycombs. *Carbon*. 2017;118:348-57.

[6] Krainyukova, Nina V. Capturing Gases in Carbon Honeycomb. *Journal of Low Temperature Physics*. 2017;187(1-2):90-104.

[7] Shi, Le, Xu, Ao, Zhao, Tianshou. Three-Dimensional Carbon-Honeycomb as Nanoporous Lithium and Sodium Deposition Scaffold. *Journal of Physical Chemistry C*. 2018;122(37):21262-8.

[8] Gao Y, Chen Y, Zhong C, Zhang Z, Xie Y, Zhang S. Electron and phonon properties and gas storage in carbon honeycombs. *Nanoscale*. 2016;8(26):12863-8.

[9] Wei Z, Yang F, Bi K, Yang J, Chen Y. Thermal transport properties of all-sp² three-dimensional graphene: Anisotropy, size and pressure effects. *Carbon*. 2017;113:212-8.

[10] Yang Z, Lan G, Ouyang B, Xu L-C, Liu R, Liu X, et al. The thermoelectric performance of bulk three-dimensional graphene. *Materials Chemistry and Physics*. 2016;183:6-10.

[11] Wang S, Wu D, Yang B, Ruckenstein E, Chen H. Semimetallic carbon honeycombs: new three-dimensional graphene allotropes with Dirac cones. *Nanoscale*. 2018;10(6):2748-54.

[12] Fthenakis ZG. Are the experimentally observed 3-dimensional carbon honeycombs all-sp² structures? The dangling p-orbital instability. *RSC Advances*. 2017;7(16):9790-4.

[13] Han Y, Yang J-Y, Hu M. Unusual strain response of thermal transport in dimerized three-dimensional graphene. *Nanoscale*. 2018;10(11):5229-38.

[14] Hu J, Wu W, Zhong C, Liu N, Ouyang C, Yang HY, et al. Three-dimensional honeycomb carbon: Junction line distortion and novel emergent fermions. *Carbon*. 2019;141:417-26.

[15] Pang Z, Gu X, Wei Y, Yang R, Dresselhaus MS. Bottom-up design of three-dimensional carbon-honeycomb with superb specific strength and high thermal conductivity. *Nano Letters*. 2016;17(1):179-85.

[16] Liu X, Guo W. Inner edge magnetisms in carbon honeycombs. *Journal of Applied Physics*. 2018;123(14):1443011-8.

- [17]Singh D, Murthy JY, Fisher TS. Mechanism of thermal conductivity reduction in few-layer graphene. *Journal of Applied Physics*. 2011;110(4):p.044317.1-8.
- [18]Zhong C, Chen YP, Xie Y, Yang S, Cohen M, Zhang S. Towards Three-Dimensional Weyl-Surface Semimetals in Graphene Networks. *Nanoscale*. 2016;8(13):7232-9.
- [19]Wang T, Wang Z, Salvatierra RV, McHugh E, Tour JM. Top-down synthesis of graphene nanoribbons using different sources of carbon nanotubes. *Carbon*. 2020;158:615-23.
- [20]Perdew JP, Burke K, Ernzerhof M. Generalized Gradient Approximation Made Simple. *Physical Review Letters*. 1996;77(18):3865-8.
- [21]Perdew JP. Density-functional approximation for the correlation energy of the inhomogeneous electron gas. *Physical Review B*. 1986;33(12):8822.
- [22]Kresse G, Furthmüller J. Efficient iterative schemes for ab initio total-energy calculations using a plane-wave basis set. *Physical Review B*. 1996;54(16):11169-86.
- [23]Blöchl PE. Projector augmented-wave method. *Physical Review B*. 1994;50(24):17953-79.
- [24]Monkhorst HJ, Pack JD. Special points for Brillouin-zone integrations. *Physical Review B*. 1976;13(12):5188-92.
- [25]Gonze X. First-principles responses of solids to atomic displacements and homogeneous electric fields: Implementation of a conjugate-gradient algorithm. *Physical Review B*. 1997;55(16):10337-54.
- [26]Li W, Carrete J, A. Katcho N, Mingo N. ShengBTE: A solver of the Boltzmann transport equation for phonons. *Computer Physics Communications*. 2014;185(6):1747-58.
- [27]Giannozzi P, Baroni S. Density-Functional Perturbation Theory. In: Yip S, ed. *Handbook of Materials Modeling: Methods*. Dordrecht: Springer Netherlands 2005, p. 195-214.
- [28]Togo A, Tanaka I. First principles phonon calculations in materials science. *Scripta Materialia*. 2015;108:1-5.
- [29]Xie H, Ouyang T, Germaneau E, Qin G, Hu M, Bao H. Large tunability of lattice thermal conductivity of monolayer silicene via mechanical strain. *Physical Review B*. 2016;93(7):075404.
- [30]Kuang Y, Lindsay L, Huang B. Unusual Enhancement in Intrinsic Thermal Conductivity of Multilayer Graphene by Tensile Strains. *Nano Letters*. 2015;15(9):6121-7.
- [31]Parrish KD, Jain A, Larkin JM, Saidi WA, McGaughey AJ. Origins of thermal conductivity

changes in strained crystals. *Physical Review B*. 2014;90(23):235201.

[32] Kuryliuk V, Nepochatyi O, Chantrenne P, Lacroix D, Isaiev M. Thermal conductivity of strained silicon: molecular dynamics insight and kinetic theory approach. *Journal of Applied Physics*. 2019;126(5):055109-.

[33] Broido D, Lindsay L, Ward A. Thermal conductivity of diamond under extreme pressure: a first-principles study. *Physical Review B*. 2012;86(11):115203.

[34] Callaway J. Model for lattice thermal conductivity at low temperatures. *Physical Review*. 1959;113(4):1046.

[35] Kantorovich L. *Quantum Theory Of The Solid State*. *Materials Today*. 2004;7(6):55.

[36] Feng Huang L, Zeng Z. Lattice dynamics and disorder-induced contraction in functionalized graphene. *Journal of Applied Physics*. 2013;113(8):083524.

[37] Huang LF, Gong PL, Zeng Z. Correlation between structure, phonon spectra, thermal expansion, and thermomechanics of single-layer MoS₂. *Physical Review B*. 2014;90(4):045409.

[38] Huang L-F, Gong P-L, Zeng Z. Phonon properties, thermal expansion, and thermomechanics of silicene and germanene. *Physical Review B*. 2015;91(20):205433.

[39] Huang L-F, Zeng Z. Roles of mass, structure, and bond strength in the phonon properties and lattice anharmonicity of single-layer Mo and W dichalcogenides. *The Journal of Physical Chemistry C*. 2015;119(32):18779-89.

[40] Verdier M, Han Y, Lacroix D, Chapuis P-O, Termentzidis K. Radial dependence of thermal transport in silicon nanowires. *Journal of Physics: Materials*. 2018;2(1):015002.